SPECIAL TOPIC — International Conference on Nanoscience & Technology, China 2013

Rational doping for zinc oxide and its influences on morphology and optical properties*

Xia Yu-Jing(夏玉静)[a)b)], Guan Zi-Sheng(管自生)[b)†], and He Tao(贺 涛)[a)‡]

[a)] National Center for Nanoscience and Technology, Beijing 100190, China
[b)] College of Materials Science and Technology, Nanjing University of Technology, Nanjing 210009, China

(Received 4 September 2013; revised manuscript received 14 March 2014; published online 10 June 2014)

Zinc oxide (ZnO) nanopowders doped with different metal ions (*Me*, *Me* = Sn^{4+}, In^{3+}, Mn^{2+}, and Co^{2+}) are prepared by a simple sol–gel method. Influences of the ion doping on morphology and optical properties of the resulting Zn_xMe_yO are investigated by scanning electron microscopy, X-ray diffraction, UV-vis absorption spectrum, and photoluminescence. The morphology of ZnO can be tailored by ion doping, which is closely related not only to the ionic radii and electronegativities of the doped ions, but also to their oxidation states and electron configurations. The optical band gap and photoluminescence of ZnO can also be modulated by ion doping, which results from a combination of different effects, Burstein–Moss, band tail, charge compensation, sp–d exchange, non-radiative recombination, and blocking barrier. This may offer us a viable approach to tuning the (optical) properties of ZnO-based materials via rational ion doping.

Keywords: zinc oxide, sol–gel chemistry, optical properties, luminescence

PACS: 77.55.hf, 78.67.Bf, 78.60.Lc, 81.20.Fw **DOI:** 10.1088/1674-1056/23/8/087701

1. Introduction

Zinc oxide (ZnO) is a semiconductor with a wide band gap ($E_g \sim 3.37$ eV, 300 K) and large excitonic binding energy (~ 60 meV). It is widely used in various optoelectronic devices due to its unique optoelectronic properties.[1,2] To realize the practical applications, many methods have been employed to optimize the properties of ZnO-based materials (such as optical, electric, and magnetic properties) in the past decades. Among them, ion doping is considered as one of the most effective approaches. The doped ZnO materials can be prepared by many physical and chemical techniques, such as evaporation,[3] pulsed laser deposition,[4] chemical vapor deposition,[5] and sol–gel method.[6] Among these techniques, the sol–gel process stands out due to its merits of low cost, simplicity, and homogeneous doping.

Since doping can have an influence on the properties of ZnO, different ions have been used to meet requirements for various applications. The high-quality, highly conductive n-type ZnO transparent films can be prepared via single-doping or co-doping of Group-III elements (such as Al, In, and Ga).[7–11] Such a thin film usually shows a high visible-light transmittance (near 90%) and a low resistivity (near 10^{-4} Ω·cm), which can be used in solar cells as transparent electrode.[12,13] Room-temperature ferromagnetism, promising for semiconductor spintronics, can be achieved by doping transition metal elements (such as Mn, Co, Fe, Ni, and V) into ZnO.[14–19]

The doping effects are usually explained in terms of ionic radii and electronegativities of the doping ions. Other factors such as oxidation states and electron configurations of the doping ions are not discussed much,[20] neither are the comprehensive effects of none of all these influencing factors. For the optical properties, in addition, different assumptions have been proposed to explain the origins of many photoluminescence (PL) emission bands observed in the visible spectral region.[21,22] Since different doping ions may introduce different defects, more information about the origin of PL emission can be collected by doping a series of metal ions into ZnO. In this work, hence, four metal ions (Sn^{4+}, In^{3+}, Mn^{2+}, Co^{2+}) are used as dopants to prepare doped ZnO nanopowders by a simple sol–gel method. These ions differ in ionic radius, electronegativity, oxidation state, and electron configuration. The influences of ion doping on microstructure, optical absorption, and PL are thoroughly discussed. We envision that these may hammer out a solid foundation on how to tune the (optical) properties of ZnO-based materials via ion doping.

2. Experiment

2.1. Preparation of doped ZnO

Zinc acetate dihydrate ($(CH_3COO)_2Zn{\cdot}2H_2O$, AR) was used as the zinc source to prepare the sol gel for differ-

*Project supported by the National Key Basic Research Program of China (Grant No. 2011CB933200), the Funds from the Ministry of Science and Technology of China (Grant No. 2010DFB63530), the National Natural Science Foundation of China (Grant Nos. 51043010 and 21071081), and the Hundred-Talent Program of Chinese Academy of Sciences.

†Corresponding author. E-mail: zishengguan@163.com
‡Corresponding author. E-mail: het@nanoctr.cn

© 2014 Chinese Physical Society and IOP Publishing Ltd

ent samples. Ethanol and monoethanolamine (MEA) were used as the solvent and stabilizer respectively. The respective dopant sources for Sn^{4+}, In^{3+}, Co^{2+}, and Mn^{2+} were tin chloride pentahydrate ($SnCl_4{\cdot}5H_2O$, AR), indium trichloride tetrahydrate ($InCl_3{\cdot}4H_2O$, AR), cobalt acetate tetrahydrate ($(CH_3COO)_2Co{\cdot}4H_2O$, AR), and manganese acetate tetrahydrate ($(CH_3COO)_2Mn{\cdot}4H_2O$, AR) respectively. The concentration of zinc ion was 0.5 M, and the molar ration of MEA to zinc ion was maintained at 1.0. The zinc acetate and one type of dopant source were first dissolved in a mixture of ethanol and MEA. For the doping of different ions, the metal-source concentrations for Sn^{4+} and In^{3+} were maintained at 1.0 at.%, 2.0 at.%, and 3.0 at.%, while those for Co^{2+} and Mn^{2+} were 1.0 at.%, 3.0 at.%, and 5.0 at.%. The doped samples (Zn_xMe_yO) were denoted as *m-Me* (such as 1-Sn, 2-Sn, 3-Sn, and 5-Mn), in which *m* refers to the atomic percentage of doping source in the starting material and *Me* denotes the dopant element. The mixture was stirred at room temperature for 3 h to yield a clear and homogeneous solution. After aging for 48 h, a gel was obtained by evaporating the solvent of resulting solution with a rotary evaporator. The resulting gel was first annealed at 450 °C for 1 h in air in an alumina crucible and then annealed at 650 °C for another 1 h.

2.2. Characterization

X-ray diffraction (XRD) patterns were acquired using a Bruker D8 Focus diffractometer (Cu Kα, $\lambda = 1.5406$ Å) in a scan range of 20°–80°. Scanning electron microscopy (SEM) image analysis was conducted with a Hitachi S-4800 at an accelerating voltage of 10 kV. Diffuse reflectance UV-vis absorption spectra (UV-vis) were collected with a UV-vis spectrometer (Lambda 750, PE). Photoluminescence (PL) spectra were recorded with a spectrofluorometer (LS 45/55). All the measurements were carried out at room temperature (25±2 °C), unless otherwise stated.

3. Results

3.1. Structural and morphological analysis

3.1.1. X-ray diffraction patterns

Crystal structure of the obtained doped-ZnO nanopowders are studied using X-ray diffraction (XRD) technique. Figure 1 shows the typical XRD patterns of all the samples. Several pronounced peaks, which can be indexed to (100), (002), and (101) crystal planes of ZnO, appear at 2θ values of 31.76°, 34.43°, and 36.26° respectively. For all the samples, the major diffraction peaks can all be indexed to the hexagonal wurtzite structure of ZnO crystal with reference to Joint Committee on Powder Diffraction Standards (JCPDS) file No. 36-1451.[23] The sharp diffraction peaks imply that all the doped-ZnO samples, as well as ZnO, have a high crystallinity each. The characteristic peaks of impurities (such as CoO_x and MnO_x) are not observed in the XRD patterns for the sample doped with Co^{2+} nor for the sample doped with Mn^{2+}, while the oxide impurity phases appear in the samples doped with Sn^{4+} and In^{3+} when the doping quantity increases to 2.0 at.% (Fig. 1).

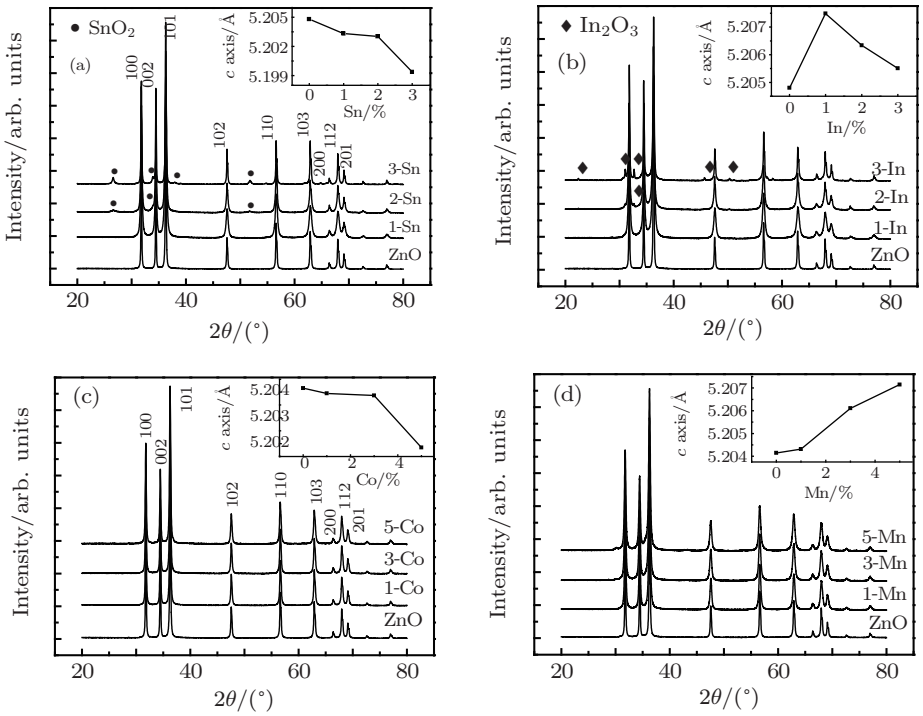


Fig. 1. XRD patterns of undoped ZnO sample and of doped ZnO samples with (a) Sn^{4+}, (b) In^{3+}, (c) Co^{2+}, and (d) Mn^{2+}. Each inset shows the variation trend of *c*-axis lattice constant with the doping quantity.

The impurity oxides can be indexed to the structures of SnO_2 and In_2O_3, for which the mass ratio can be roughly determined using reference-intensity-ratio (RIR) method (Table 1). It is noted that although the RIR method gives a pretty large error here, the trend for change in the quantity of impurity oxides can clearly be seen. Thus, the quantity of impurity oxides increases as the doping quantities of Sn^{4+} and In^{3+} ions increase. The evolutions of such impurity oxides also explain why in this work the highest doping quantities for Sn^{4+} and In^{3+} ions are lower than those for Co^{2+} and Mn^{2+} ions.

In addition, the crystallite sizes of the samples are determined using the diffraction peaks with Scherrer equation,[24] which are summarized in Table 1. It is found that the crystallite sizes for all the doped samples are smaller than that for ZnO sample. This indicates that the doping can inhibit the growth of ZnO crystal. Moreover, the crystallite sizes decrease gradually with increasing the doping quantities for the samples doped with Co^{2+} and Mn^{2+}, while for the samples doped with Sn^{4+} and In^{3+} they increase with increasing the doping quantity.

Table 1. Crystallite sizes and mass ratios of impurity oxides for *Me*-doped samples.

	Crystallite size/nm					Ratio/wt%	
	0 at.%	1 at.%	2 at.%	3 at.%	5 at.%	2 at.%	3 at.%
Sn^{4+}-doped ZnO	80.3	31.8	43.5	71.5	–	2.8	18.9
In^{3+}-doped ZnO	80.3	25.1	32.3	76.5	–	2.3	5.5
Co^{2+}-doped ZnO	80.3	53.3	–	52.5	47.5	–	–
Mn^{2+} doped ZnO	80.3	33.8	–	28.9	27.6	–	–

3.1.2. Scanning electron microscopy images

Changes in the grain size of the samples induced by ion doping are studied by scanning electron microscopy (SEM) technique. The SEM results indicate that the grain sizes for all the doped samples are smaller than that for ZnO sample, suggesting the suppression of crystal growth by doping. This accords well with the XRD results. Figure 2 shows typical SEM images of undoped ZnO sample and the doped samples (Zn_xMe_yO) with a doping amount of 3.0 at.%. The particles for both ZnO sample and doped samples exhibit sphere-like morphologies. It can be observed that for pure ZnO, most of particles have grain sizes of about 120 nm, while some of them have the grain sizes larger or smaller than that value. For 3-Sn and 3-In samples, however, an abnormal growth phenomenon is observed in the images, i.e., coalescence of particles occurs, and nano-flakes or nano-sheets are formed besides the nanoparticles. This cannot be observed when the doping quantities of Sn^{4+} and In^{3+} ions are low such as 1.0 at.% (see the insets of Fig. 2). It is noted that such an abnormal growth is not observed in 3-Co sample nor 3-Mn sample. As indicated by XRD results (Fig. 1), in addition, for Sn^{4+}- and In^{3+}-doped samples the impurity phase can be observed only for those with a high doping quantity (3-Sn and 3-In), while impurity phase can be observed for neither Co^{2+}-nor Mn^{2+}-doped samples regardless of their doping quantities. Hence, it is reasonable to conclude that this phenomenon is closely related to the evolved impurity phase, which can serve as nucleation centers. This has been evidenced by the literature that shows that the high concentration of dopant can cause the coalescence of nanorods.[25] The study for detailed mechanism is still under way.

3.2. Photophysics

3.2.1. UV-Vis absorption spectra

Figure 3 shows room-temperature optical absorption spectra of undoped and doped samples. A strong absorption in the UV region can be observed for all of the samples, which is attributed to the band-to-band transition. The band gap energy (E_g) can be determined using equation $\alpha = A(h\nu - E_g)^{n/2}/h\nu$, where α is the absorption coefficient, A is a constant, $h\nu$ is the photon energy.[26] Here the value of n is 1 for all of the samples since ZnO is a direct band gap semiconductor. Thus, E_g can be determined by plotting room-temperature data for $(\alpha h\nu)^2$ as a function of ($h\nu$–E_g) and extrapolating its straight line part towards zero absorption (crossing at the horizontal axis, see the insets of Fig. 3). It is found that for the Sn-doped samples, blue shift occurs in the optical band gap when the doping quantities are 1.0 at.% and 2.0 at.%, while red shift happens for a doping quantity of 3.0 at.% (see the inset of Fig. 3(a)). Similarly, blue shift takes place for In^{3+}-doped samples when the doping quantity is 1.0 at.%, and red shift occurs when the doping quantities increase to 2.0 at.% and 3.0 at.% (see the inset of Fig. 3(b)). An obvious red shift occurs for all of the Co^{2+}-doped samples, and the shift amplitude increases with the doping quantity increasing (see the inset of Fig. 3(c)). For all of the Mn^{2+}-doped samples, the shift amplitude is so small that it can hardly be recognized (see the inset of Fig. 3(d)).

Compared with undoped ZnO sample, all of the doped samples exhibit their own visible-light response, which increases with the increase of doping quantity for almost all of the samples except 2-Sn sample. This is a typical absorption feature of doped ZnO, which arises from the introduction of doping energy levels. For Co^{2+}-doped samples, in addition, three absorption peaks appear at 567, 600, and 656 nm in the spectra, which also increase with the increase of doping quantity. This is ascribed to the d–d transition of doped Co^{2+}.[23]

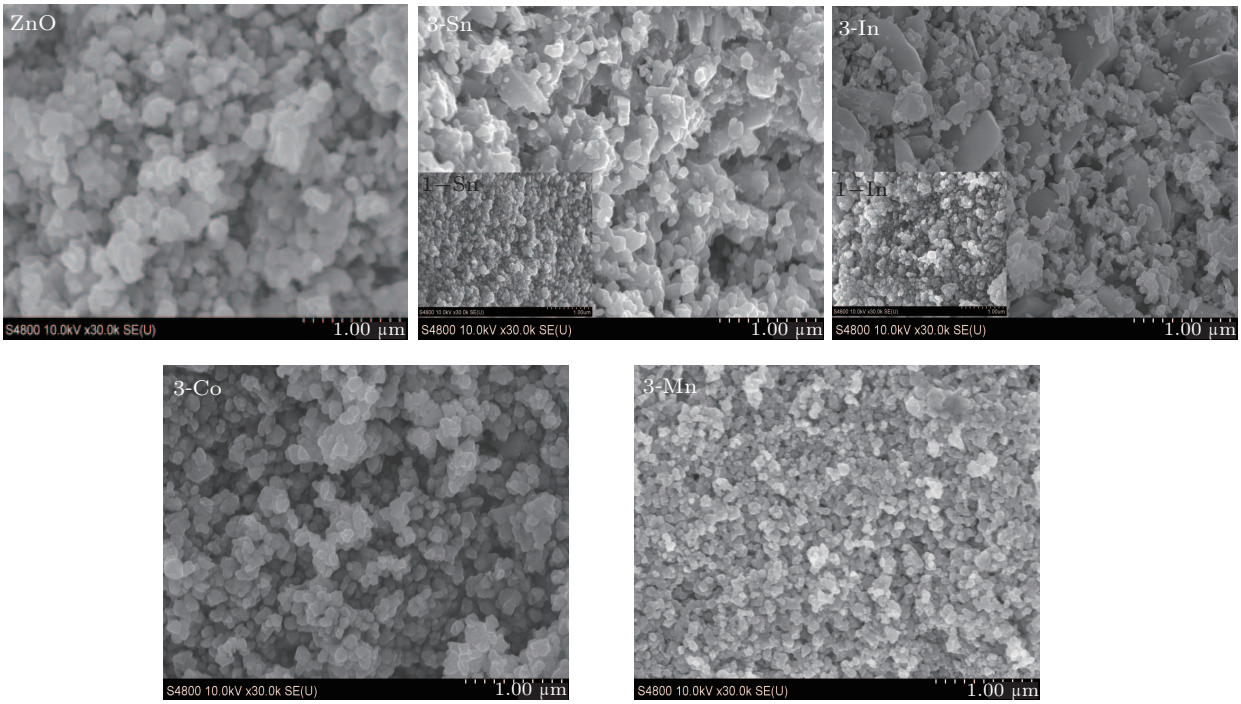


Fig. 2. Typical SEM images of undoped ZnO sample and Zn_xMe_yO samples with a doping amount of 3.0 at.%. Insets show the SEM images for the Sn- and In-doped samples each with a doping quantity of 1.0 at.%.

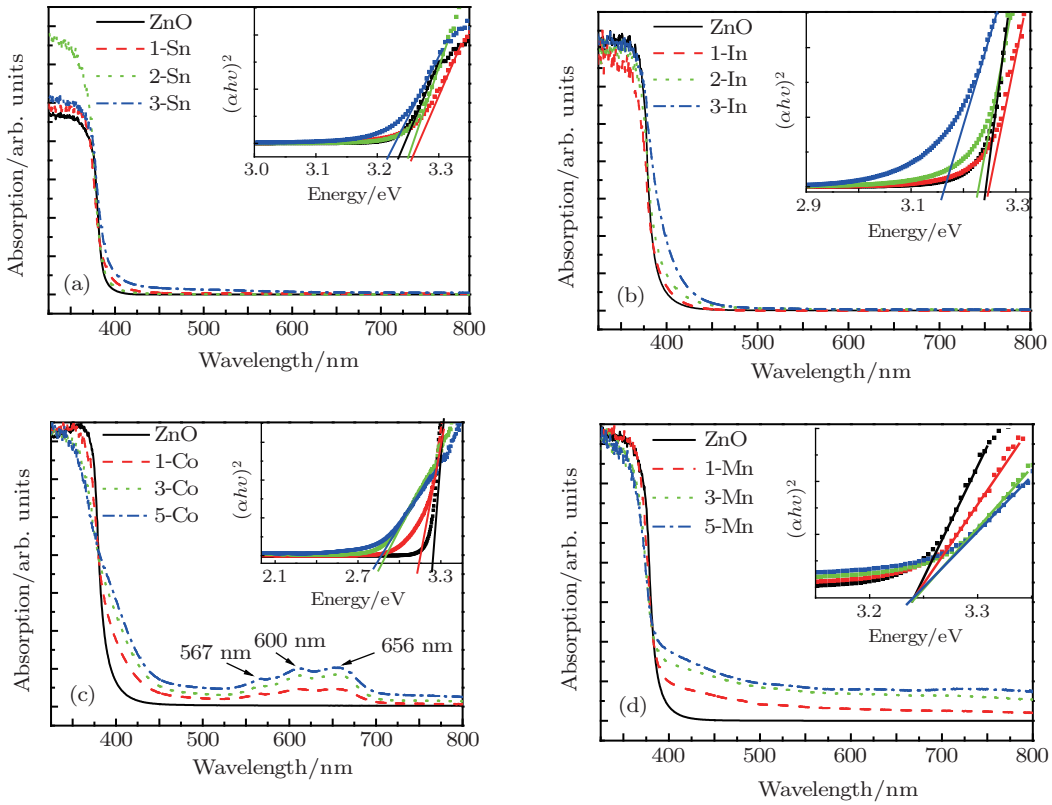


Fig. 3. (color online) UV-vis absorption spectra of undoped ZnO sample and the doped samples with (a) Sn^{4+}, (b) In^{3+}, (c) Co^{2+}, and (d) Mn^{2+}. The insets show the derivations of band gap.

3.2.2. Photoluminescence spectra

The concentration of defects on the surface is usually higher than that in the bulk. A high surface area of the nanostructure can result in an increased density of non-radiative and/or radiative defects.[22] It is known that doping can have an obvious influence on the defects and these defects are

closely related to the PL properties of a sample. Figure 4 shows the PL spectra of all the samples, for which the excitation wavelength is 325 nm. Five emission peaks appear in the spectra at 420 nm (2.95 eV), 442 nm (2.81 eV), 485 nm (2.55 eV), 497 nm (2.49 eV), and 526 nm (2.38 eV) respectively. Although the PL properties of ZnO have been widely studied, controversy still exists about the origin of these emission peaks.[21] It is accepted that emission peaks in the visible region originate from the defects in ZnO. The 420-nm emission peak has also been observed in some special ZnO nanostructures, such as nanowires and nanobelts, which is attributed to the interstitial Zn, oxygen vacancies, or interface traps.[21] The emission peak at about 440 nm is ascribed to the oxygen vacancies, possibly V_O.[27] For the green emission peak around 500 nm, it is attributed to the recombination of a photogenerated hole with an electron in a singly ionized oxygen vacancy,[28] or to the transition between conduction band and zinc vacancy.[21] The emission peak near 520 nm is ascribed to anti-oxygen,[29] oxygen vacancy, or zinc interstitial.[30] It is noted that single-crystal ZnO often contains metal excess or oxygen deficiency, which can be accommodated in part by the presence of zinc interstitials or oxygen vacancies. Since there is still controversy about which of these is the predominant defect, the effects of metal excess as well as oxygen deficiency need to be studied in future.

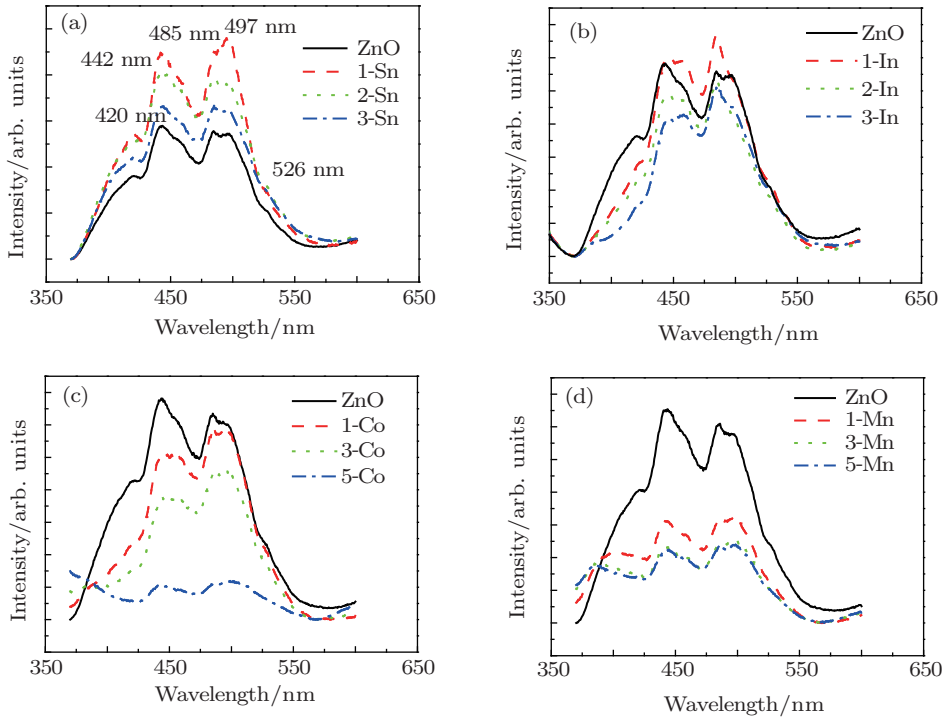


Fig. 4. (color online) PL spectra of undoped ZnO sample and doped ZnO samples with (a) Sn^{4+}, (b) In^{3+}, (c) Co^{2+}, and (d) Mn^{2+}.

No major emission peaks disappear in the PL spectra for any of the doped samples, neither does a new peak appear. The PL intensity is higher for all of the Sn^{4+}-doped samples than for the undoped ZnO sample, while it is lower for all of the Co^{2+}- and Mn^{2+}-doped samples. Except the peak at 420 nm, the PL intensity is higher for In^{3+}-doped samples than that for undoped ZnO sample when the doping amount is 1.0 at.%, while it is lower when the doping amount increases to 2.0 at.% and 3.0 at.%. It is noted that the peak intensity of PL emission decreases with the increase of the doping amount for all of the doped samples (Fig. 4).

4. Discussion

4.1. Doping mechanism

Many factors can have an influence on doping ions into ZnO. Electronegativity and ionic radius are the two factors that are often considered. If the electronegativities and ionic radii of the doping metal ions match those of the lattice metal ions in the oxide, the lattice metal can be substituted by the doping ions during preparation. Since the electronegativities and ionic radii of Sn^{4+} (1.96, 71 pm),[31] In^{3+} (1.78, 81 pm),[11] Co^{2+} (1.88, 72 pm),[32] and Mn^{2+} (1.55, 80 pm)[32] are close to those of Zn^{2+} (1.65, 74 pm),[31] it is expected that these metal ions can occupy the lattice Zn^{2+} positions in ZnO. However, since the values of electronegativity and ionic radius of those

doped ions are different from each other, though only slightly, the doping effects can be different between them.

It is known that lattice distortion can occur in crystal by ion doping, leading to an increase in the internal energy of ZnO system. The doped ions with larger radii tend to occupy the grain boundaries of expansion lattices, and those with smaller radii tend to occupy the grain boundaries of compression lattices. This segregation process can reduce the internal energy. Hence, the concentration of doped ions at the grain boundary is higher than that in the bulk. These enriched ions at the grain boundary can form a diffusion barrier, which can suppress the growth of ZnO crystal. This can explain why all of the doped samples each have a smaller crystallite size than the undoped ZnO sample.

As the doping amount increases, nucleation probability of impurity phase increases accordingly. Once the doping amount reaches a limit, this can lead to the formation of impurity oxides for the enriched doped ions at the grain boundary. In addition, the oxidation states of Sn^{4+} and In^{3+} ions are different from that of Zn^{2+}. This can further enhance the lattice distortion, which can make the doped ions emerge from the ZnO lattice, producing the evolution of impurity oxides (SnO_2 and In_2O_3) when the doping quantity is high enough (such as 2.0 at.%). Since Sn^{4+} has a higher oxidation state than In^{3+} ion, the quantity of evolved SnO_2 is more than that of In_2O_3 at the same 'doping' quantity (Table 1). As for Co^{2+} and Mn^{2+} ions, they have the same oxidation state as Zn^{2+}. This makes them match the lattice Zn^{2+} ions preferably, which may be the reason why no impurity oxides are observed for Co^{2+}-doped sample nor Mn^{2+}-doped samples in our experiments even at a relatively high doping quantity (such as 5.0 at.%). This implies that it is easy to form impurity phase when the doped ions have a higher (different) oxidation state than the lattice ions. For the samples doped with Co^{2+} and Mn^{2+}, the inhibition effect on grain growth increases with the increase of doping quantity and, accordingly, the crystallite size gradually decreases with increasing the doping quantity (Table 1). While for the samples doped with Sn^{4+} and In^{3+}, more and more dopants can exist in the form of impurity oxides with the increase of doping quantity. Hence, the inhibition effect may decrease with increasing the doping quantity, and therefore the crystallite size increases with the increase of doping quantity (Table 1). Here the effects from acetates (especially in terms of the surface energetics) are not discussed as the zinc acetate is used for preparing all the samples, for which the concentration is much higher (0.5 M) than any of the dopants used in the starting material (the highest one is 5.0 at.%). It would thus be reasonable to assume the effects from acetates to be the same for all of the samples.

The lattice parameters can also be used to study the doping effects, which can be deduced from the XRD data.[33] However, the changes in them (here, *c*-axis lattice constant) are very small in this work (see the insets of Fig. 1), which may be because the doping quantity in substitutional mode is relatively small. Thus, the change in *c*-axis lattice constant is no longer discussed in this work, although it usually decreases in the case of doped ions with smaller ionic radii (such as Sn^{4+} and Co^{2+}) as they tend to occupy the grain boundaries of the compression lattices and it usually increases for the doped ions with larger ionic radii (such as In^{3+} and Mn^{2+}) as they tend to occupy grain boundaries of the expansion lattices.

4.2. Influences of doping on photophysical properties

4.2.1. UV-vis absorption

Doping can have a huge influence on the photophysical properties of ZnO. At a high doping density, the concentration of point defects induced by ion doping increases. Meanwhile, the formation of solid solution also increases. Hence, the wave function of donors can overlap with each other, resulting in a distribution of states. The Urbach band tail is thus formed in the band gap.[34] This can cause a number of possible transitions to be allowed, such as band to tail and tail to tail. Accordingly, this band-tail effect can lead to a red shift of the optical band gap. In addition, the defect levels in the band gap are isolated at a low doping density. The donor electrons can enter into the bottom of the conduction band, thereby occupying the orbits. According to the Pauli's principle, two electrons that occupy the same orbit should have different spinning directions. The low energy transition can thus be suppressed. As a result, the band gap widens, i.e. blue shift happens. This is the Burstein–Moss effect (B–M effect, or band-filling effect).[35] Here the quantum-size effect is not considered as the crystallite size, for all the samples are much larger than 10 nm in size.[36,37]

Moreover, the doped ions with a higher oxidation state than the lattice ions can lead to an increase in the charge-carrier density. The higher the oxidation state, the larger the increase is. It is noted that Sn^{4+} ions have the highest oxidation states, followed by In^{3+} ions, Co^{2+} and Mn^{2+} ions as well as the lattice Zn^{2+} ions that are in the lowest states. Therefore, for different doping ions, their effect (B–M or band tail) starting to play a major role may take place at different doping quantities. Given that the actual doping quantities in ZnO are the same, the B–M effect may be stronger for the doped ions with higher oxidation states than with lower oxidation states, as the former can afford more charge carriers; while for a higher doping amount the band-tail effect (i.e., red shift) is expected to play a major role.

The observed phenomena can thus be explained in terms of the aforementioned mechanism. For the Sn^{4+}- and In^{3+}-doped samples, the B–M effect plays a major role at a low doping quantity (such as 1.0 at.%), leading to a blue shift in the band gap. When the doping reaches a relatively high quantity, it is the band-tail effect that plays a major role, which can cause a red shift in the band gap. It is noted that the red shift occurs, starting from 3.0 at.% for Sn^{4+}-doped samples, while for In^{3+}-doped samples it starts from 2.0 at.%. This may be because Sn^{4+} ions have higher oxidation states than In^{3+} ions as discussed above.

As the oxidation state of Co^{2+} is identical to that of Zn^{2+}, the substitution of Zn^{2+} by Co^{2+} ions would not produce or consume additional charge carriers. Hence, the B–M effect may play a weaker role than the band-tail effect. Moreover, since Co is a transition-metal element and it has unfilled d orbitals, a strong sp–d exchange can occur upon doping between the band electrons of ZnO and the localized d electrons of Co^{2+}.[23] The s–d and p–d exchange interactions can cause a negative and a positive correction respectively with the edge of conduction and valence band, resulting in a band gap narrowing.[23] Together with the band-tail effect, therefore, red shift occurs in the band gap for all of the Co^{2+}-doped samples, and the shift amplitude increases with the doping quantity increasing.

While for an Mn^{2+}-doped sample, though it has an identical oxidation state to Co^{2+} and Zn^{2+}, it has a much weaker sp–d exchange effect than Co^{2+} since it has a stable electron configuration of $[Ar]3d^5$ and Co^{2+} does not ($[Ar]3d^7$). In addition, the band-tail effect for Mn^{2+} ions may also be very weak, possibly because it has the lowest electronegativity among all the elements reported here. Hence, for Mn^{2+}-doped samples, the B–M effect may approximately offset the effects of band tail and sp–d exchange, leading to almost no shift in the band gap.

In addition, characteristic absorption peaks are observed in the visible-light region for all of the doped samples, which are due to the d–d electronic transition between split 3d levels in ZnO crystal field. Moreover, the major d–d transitions occur at the energy levels of $^6A_1 \rightarrow {}^4T_1$, $^4T_2$, $^4A_1$, and 4E for Mn^{2+}-doped samples,[38] corresponding to the absorption peak around 400 nm $\sim$ 500 nm. For the Co^{2+}-doped samples, the three characteristic absorption peaks at 567, 600, and 656 nm correspond to the d–d transitions of $^4A_2(F) \rightarrow {}^2E(G)$, $^4A_2(F) \rightarrow {}^4T_1(P)$, $^4A_2(F) \rightarrow {}^2A_1(G)$, respectively.[23]

4.2.2. Photoluminescence emission

After electrons are excited from valence band to conduction band upon irradiation, they can first fall into the defects (such as oxygen vacancy) from the conduction band via a non-radiative process, then recombine with the holes in valence band, accompanied by PL emission. The non-radiative process mainly includes phonon emission and Auger recombination and is closely related to the defects of material. Hence, a decrease in the PL intensity indicates a decrease in the recombination rate, and thus an enhanced charge separation efficiency of photoinduced electrons and holes. It is known that the doping of ions can increase the defect density, leading to an influence on the PL property.

Since Sn^{4+} and In^{3+} ions each have a higher oxidation state than Zn^{2+} ions, the charge compensation can induce more structural defects (such as oxygen vacancies and zinc vacancies) upon doping, which can contribute to the PL emission. Considering the fact that Sn^{4+}-doped TiO_2 has a lower intensity of PL emission than undoped TiO_2,[39] this charge-compensation effect may be the major reason why the intensity of PL emission for the samples doped with Sn^{4+} and In^{3+} is enhanced at a doping quantity of 1.0 at.% compared with for the undoped ZnO. Another possible reason is that the grain size becomes smaller for the samples doped with small quantities of Sn^{4+} and In^{3+}. This will lead to a larger specific surface area, and thus more defects such as oxygen vacancies and surface states. Some of these defects can contribute to the PL emission.

It is noted that the aforementioned enrichment of doped ions at the grain boundary can lead to the formation of a blocking barrier, resulting in suppression of the recombination of photogenerated electrons and holes.[40] This blocking effect increases with the increase of doping quantity. When the doping quantity reaches a limit, the impurity oxide emerges in Sn^{4+}- and In^{3+}-doped samples. The higher the doping quantity, the more the formed impurity oxides are. This impurity oxide formed on the surface of the doped ZnO has a potential energy large enough to prevent the surface states from trapping photogenerated charges carriers.[40] As discussed above, moreover, doping Sn^{4+} and In^{3+} ions into ZnO lattice can lead to an increase in the charge–carrier density and the formation of band tail, which increase with increasing the doping quantity. This can give rise to an enhancement of non-radiative recombination (such as Auger recombination).[41] Furthermore, the grain sizes of doped samples increase with increasing the doping quantities of Sn^{4+} and In^{3+} ions, resulting in a reduction of surface defects. All these effects can result in a fluorescence quenching, and thus can explain why the peak intensity of PL emission decreases gradually with the increase of the doping quantities of Sn^{4+} and In^{3+} ions.

In addition, Sn^{4+} ions have a larger charge-compensation effect than In^{3+} ions as it has a higher oxidation state. Based

on the aforementioned discussion, this may explain why for all of the Sn^{4+}-doped samples the PL intensity is higher than for the undoped ZnO, while for In^{3+}-doped samples it is lower than for ZnO when the doping amounts increase to 2.0 at.% and 3.0 at.% respectively.

Unlike Sn^{4+} and In^{3+} dopants, doping Co^{2+} and Mn^{2+} cannot provide excess electrons. Thus, neither the charge-compensation effect nor the enhancement of non-radiative Auger recombination is expected. It is noted that doping Co^{2+} and Mn^{2+} ions can lead to the formation of deep doping energy levels in ZnO which are located near Fermi level.[42] So it is suggested that multi-phonon emission can occur between isolated doping levels inside the band gap, resulting in non-radiative recombination. This may explain why the PL emission intensity is lower for all of the Co^{2+}- and Mn^{2+}-doped samples than for the undoped ZnO. In addition, the strong quenching effect for the peak at 420 nm may be caused by the non-radiative recombination such as multi-phonon emission. Like the Sn^{4+}- and In^{3+}-doped samples, the blocking effect due to the enrichment of doped ions at the grain boundary is the major reason why the fluorescence quenching increases with the increase of doping quantities of Co^{2+} and Mn^{2+} ions.

Moreover, with respect to other emission peaks, it is found that the emission around 526 nm does not change significantly with increasing the doping quantities for the Sn^{4+}- and In^{3+}-doped samples, while the changing trends of this peak for the Co^{2+}- and Mn^{2+}-doped samples are consistent with those of the other emission peaks. Since this peak is ascribed to the anti-oxygen, it is suggested that doping ions with higher oxidation states than the lattice ions may increase the concentration of anti-oxygen atoms. The lattice strain may thus be cancelled out, result in almost no change in the PL emission intensity with the change in doping quantity.

It is noted that the fluorescence is strongly quenched at a doping quantity of 1.0 at.% for Mn^{2+}-doped samples, while for Co^{2+}-doped samples it occurs at a doping amount of 5.0 at.%. This may be because the grain sizes for Mn^{2+}-doped samples are smaller than those for Co^{2+}-doped samples. Hence, more defects that can contribute to the fluorescence quenching are present in Mn^{2+}-doped samples than in Co^{2+}-doped samples. Another possible reason may be related to the electron configuration and the effect of sp–d exchange of Co^{2+} and Mn^{2+} ions. Further study is required to elucidate this.

5. Conclusion

The influences of ion doping on the crystal morphology, optical absorption, and PL emission of ZnO are studied systematically via doping with four different ions (Sn^{4+}, In^{3+}, Co^{2+}, and Mn^{2+}). These ions differ in many properties, such as ionic radius, electronegativity, oxidation state, and electron configuration, which can have an influence on the doping behaviors of the ions, leading to different micro-structures and morphologies of the resulting crystals. The optical absorptions of the resulting doped samples are determined by many factors, such as band-tail effect, Burstein–Moss effect, and sp–d exchange effect. The band-tail effect and Burstein–Moss effect can be changed with the doped ion number when the oxidation states are different from those of the lattice ions. The sp–d exchange effect is closely related to the electron configuration of the doped ions. The oxidation state of the doped ions can also have an influence on their enrichment at the grain boundary, which can influence the crystal growth. Similarly, the PL emissions of the doped samples are also the comprehensive consequences of many influencing factors, such as charge compensation (closely related to oxidation state of the doped ions), blocking barrier (due to the enrichment of doped ions and the evolution of impurity oxide at the grain boundary), non-radiative recombination, and possibly also the sp–d exchange effect. In addition, it is noted that grain boundary and interface of nanomaterials may have an influence on the properties of doped ZnO too, on which the research is under way. Nevertheless, all these can be used for a rational synthesis of doped ZnO so as to tailor the properties of ZnO-based materials, which may present a viable approach for related real applications.

References

[1] Özgur Ü, Alivov Y I, Liu C, Teke A, Reshchikov M A, Dogan S, Avrutin V, Cho S J and Morkoc H 2005 *J. Appl. Phys.* **98** 041301
[2] Wang Z L 2004 *J. Phys.: Condens. Matter* **16** R829
[3] Li L J, Yu K, Wang Y and Zhu Z Q 2010 *Appl. Surf. Sci.* **256** 3361
[4] Holmelund E, Schou J, Tougaard S and Larsen N B 2002 *Appl. Surf. Sci.* **197–198** 467
[5] Ben Yaacov T, Ive T, van de Walle C G, Mishra U K, Speck J S and Denbaars S P 2010 *J. Electron. Mater.* **39** 608
[6] Kima Y S and Tai W P 2007 *Appl. Surf. Sci.* **253** 4911
[7] Gaspera E D, Bersani M, Cittadini M, Guglielmi M, Pagani D, Noriega R, Mehra S, Salleo A and Martucci A 2013 *J. Am. Chem. Soc.* **135** 3439
[8] Buonsanti R, Llordes A, Aloni S, Helms B A and Milliron D J 2011 *Nano Lett.* **11** 4706
[9] Kuo S Y, Chen W C, Lai F I, Cheng C P, Kuo H C, Wang S C and Hsieh W F 2006 *J. Cryst. Growth* **287** 78
[10] Ratana T, Amornpitoksuk P, Ratana T and Suwanboon S 2009 *J. Alloys Compd.* **470** 408
[11] Ahmad M, Zhao J, Iqbal J, Miao W, Xie L, Mo R and Zhu J 2009 *J. Phys. D: Appl. Phys.* **42** 165406
[12] Bhosle V, Prater J T, Yang F, Burk D, Forrest S R and Narayan J 2007 *J. Appl. Phys.* **102** 023501
[13] Matsubara K, Fons P, Iwata K, Yamada A, Sakurai K, Tampo H and Niki S 2003 *Thin Solid Films* **431–432** 369
[14] Straumal B, Mazilkin A, Protasova S, Myatiev A, Straumal P, Goering E and Baretzky B 2011 *Phys. Stat. Sol. B* **248** 1581
[15] Straumal B B, Mazilkin A A, Protasova S G, Myatiev A A, Straumal P B, Goering E and Baretzky B 2011 *Thin Solid Films* **520** 1192
[16] Wu D W, Huang Z B, Yin G F, Yao Y D, Liao X M, Han D, Huang X and Gu J W 2010 *Cryst. Eng. Comm.* **12** 192

[17] Park J H, Kim M G, Jang H M, Ryu S and Kim Y M 2004 *Appl. Phys. Lett.* **84** 1338
[18] Janisch R, Gopal P and Spaldin N A 2005 *J. Phys.: Condens. Matter* **17** 657
[19] Pan F, Song C, Liu X J, Yang Y C and Zeng F 2008 *Mater. Sci. Eng. R* **62** 1
[20] Singh S and Rao M S R 2009 *Phys. Rev. B* **80** 045210
[21] Djurisic A B and Leung Y H 2006 *Small* **2** 944
[22] Djurisic A B, Ng A M C and Chen X Y 2010 *Prog. Quantum Electron.* **34** 191
[23] Maensiri S, Sreesongmuang J, Thomas C and Klinkaewnarong J 2006 *J. Magn. Magn. Mater.* **301** 422
[24] Cullity B D 1978 *Elements of X-Ray Diffraction*, 2nd edn. (London: Addison-Wesley Publishing Company Inc.)
[25] Yang J, Lee J, Im K and Lim S 2009 *Physica E* **42** 51
[26] Chattopadhyay S, Dutta S, Banerjee A, Janaa D, Bandyopadhyay S, Chattopadhyay S and Sarkar A 2009 *Physica B* **404** 1509
[27] Vanheusden K, Seager C H, Warren W L, Tallant D R and Voigt J A 1996 *Appl. Phys. Lett.* **68** 403
[28] Yu W D, Li X M and Gao X D 2005 *Cryst. Growth Des.* **5** 151
[29] Lin B, Fu Z and Jia Y 2001 *Appl. Phys. Lett.* **79** 943
[30] Liu X, Wu X H, Cao H and Chang R P H 2004 *J. Appl. Phys.* **95** 3141
[31] Yung K C, Liem H and Choy H S 2009 *J. Phys. D: Appl. Phys.* **42** 185002
[32] Gu Z B, Lu M H, Wang J, Du C L, Yuan C S, Wu D, Zhang S T, Zhu Y Y, Zhu S N and Chen Y F 2006 *Thin Solid Films* **515** 2361
[33] Kim K C, Kim E K and Kim Y S 2007 *Superlatt. Microstruct.* **42** 246
[34] Caglar M, Ilican S and Caglar Y 2009 *Thin Solid Films* **517** 5023
[35] El Mir L, Ben Ayadi Z, Saadoun M, Djessas K, von Bardeleben H J and Alaya S 2007 *Appl. Surf . Sci.* **254** 570
[36] Wood A, Giersig M, Hilgendorff M, Vilas-Campos A, Liz-Marzan L M and Mulvaney P 2003 *Aust. J. Chem.* **56** 1051
[37] Bouvy C, Marine W, Sporken R and Su B L 2006 *Chem. Phys. Lett.* **428** 312
[38] Wang Y S, Thomas P J and O'Brien P 2006 *J. Phys. Chem. B* **110** 21412
[39] Cao Y Q, He T, Chen Y M and Cao Y A 2010 *J. Phys. Chem. C* **114** 3627
[40] Bhargava R, Sharma P K, Dutta R K, Kumar S, Pandey A C and Kumar N 2010 *Mater. Chem. Phys.* **120** 393
[41] Maiti U N, Ghosh P K, Nandy S and Chattopadhyay K K 2007 *Physica B* **387** 103
[42] Shinde V R, Gujar T P, Lokhande C D, Mane R S and Han S H 2006 *Mater. Chem. Phys.* **96** 326